Building and Environment 242 (2023) 110429

Contents lists available at ScienceDirect

Building and Environment

journal homepage: www.elsevier.com/locate/buildenv

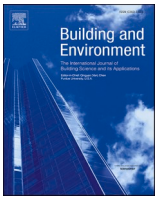

Experiment and numerical investigation of a novel flap fin louver windcatcher for multi-directional natural ventilation and passive technology integration

Jiaxiang Li [a,*], John Kaiser Calautit [a], Carlos Jimenez-Bescos [b]

[a] Department of Architecture and Built Environment, University of Nottingham, UK
[b] School of Built and Natural Environment, University of Derby, UK

ARTICLE INFO

Keywords:
Buildings
CFD
Natural ventilation
Experimental field testing
Indoor air quality
Passive cooling and heating
Windcatcher
Wind tower
Wind tunnel

ABSTRACT

Natural ventilation devices such as windcatchers are incorporated into the building design to provide fresh air supply, energy consumption reduction and, in some cases, indoor thermal comfort. However, unfavourable weather conditions limit the operation period of windcatchers, and researchers have explored the integration of passive/low-energy heating, cooling and dehumidification technologies to address this issue. While previous works have addressed the cooling or pre-heating of the supply air, most have not investigated the impact of changing wind conditions which, in some cases, render the windcatcher ineffective. Thus, a novel windcatcher with inlet openings equipped with flap fins was proposed to provide a fresh air supply irrespective of the wind direction and allow for passive/low-energy technology integration. Inspired by the check valve device, the flap fin mechanism allows wind to flow only one way into the windcatcher's supply channel. Hence, changing wind directions would not affect the ventilation rate and the location of the supply and return channels, so passive technologies can be applied effectively. The lightweight flap fin operates via gravity and takes advantage of the wind pressure around the openings to control the airflow. An open wind tunnel and test room were developed to experimentally evaluate the ventilation performance of the proposed windcatcher prototype, and a validated Computational Fluid Dynamic (CFD) model was developed. The results showed that the ventilation performance of the flap fin louver windcatcher was independent of the wind direction in the field test and wind tunnel experiment, and the use of lighter and longer fins would enhance the ventilation rate.

1. Introduction and literature review

1.1. Background and motivation

Because of the rising energy prices and concerns about global warming, researchers are exploring solutions to achieve energy efficiency in different sectors. The built environment is seen as one of the key sectors which can significantly contribute to achieving a sustainable energy economy. The construction and built environment industries are responsible for over 40% of the direct and indirect global carbon emissions [1]. While over half of the energy consumption in the building comes from the usage of heating, ventilation and air-conditioning (HVAC) systems [2,3]. Air-conditioning is one of the fastest growing energy use in the built environment and places enormous strain on the electricity grid in many parts of the world. In 2016 about 10% of the global electricity was used for cooling [4], and in cities like Shanghai with hot climates, the cooling energy consumption could reach up to 40% of the total energy load [5]. Thus, an effective cooling solution with low energy consumption needs to be investigated for low-carbon development [6].

Researchers are looking for sustainable and economical solutions to provide building occupants with good indoor thermal comfort and air quality while minimizing the use of air-conditioners [7]. There are many technology options for enhancing the building's performance. Natural ventilation is an attractive solution and has been the focus of many research studies. This is due to its capability to provide a fresh air supply and heat, moisture and pollutants removal from the building by using only the natural forces of the wind and thermal buoyancy [8]. However, natural ventilation is typically insufficient to provide the required indoor thermal comfort in unfavourable hot and cold climatic conditions. For example, in hot and humid climates, the high outdoor temperature

* Corresponding author.
E-mail addresses: Jiaxiang.li@nottingham.ac.uk (J. Li), john.calautit1@nottingham.ac.uk (J.K. Calautit).

https://doi.org/10.1016/j.buildenv.2023.110429
Received 29 January 2023; Received in revised form 13 May 2023; Accepted 16 May 2023
Available online 24 May 2023

Nomenclature

Gb	Generation of turbulence kinetic energy due to buoyancy
Gk	Generation of turbulence kinetic energy due to mean velocity gradients
p	Pressure (Pa)
Sk	User defined source term for turbulence kinetic energy (m^2/s^2)
S_ε	User defined source term for energy dissipation rate (m^2/s^3)
t	Time (s)
u	Velocity (m/s)
$\overline{V}$	Average airflow velocity in the return duct (m/s)
V_c	Airflow velocity in the centre of the return duct (m/s)
Y_M	Fluctuating dilatation in compressible turbulence to the overall dissipation rate
α_k	Inverse effective Prandtl numbers for k
α_ε	Inverse effective Prandtl numbers for ε
μ	Dynamic molecular viscosity (Pa s)
ρ	Density (kg/m^3)
τ_t	Divergence of the turbulence stress

Abbreviations

ASCD	Anti-short circuit device
CFD	Computational Fluid Dynamics
EAHE	Earth-Air Heat Exchanger
HVAC	Heating, ventilation and air-conditioning
PPM	Parts per million

and humidity in both daytime and nighttime could further cause thermal discomfort to the occupants [9,10]. This has led researchers to explore alternative solutions, such as combining natural ventilation with other passive/low-energy strategies, including solar heating, heat recovery, cooling and dehumidification [11,12].

A good example is a windcatcher, a natural ventilation device integrated with the rooftop design to capture the wind from higher levels and bring in fresh air supply while extracting polluted air similar to that of a mechanical ventilation system [13,14]. Some traditional windcatchers only have one opening for fresh air supply, and the system has to operate with windows or other openings as an outlet [15]. The multiple-opening windcatchers are more efficient as they can capture wind flow from different wind directions [16]. The windcatcher takes advantage of the natural wind forces surrounding it, as shown in Figure (1a). The positive pressure at the windward side of the windcatcher drives the supply airflow. While the negative pressure at the leeward side and sides of the windcatcher extracts the polluted air out of the building [7]. The pressure difference between the inlet and outlet openings should be maximized for optimum fresh air supply [17,18].

To enhance thermal performance, low-energy and passive technologies were incorporated with windcatchers, such as evaporative cooling, heat pipes and thermal mass. In the desert area with hot and dry summers, evaporative cooling was established to be an effective passive cooling method, but the water resource should also be considered [19–21]. The windcatcher can also be combined with a solar wall to achieve better ventilation performance [22]. Evaporative cooling and humidification were also applied in a natural ventilation system using a solar-wall-assisted windcatcher [23]. Some of the research also investigated the performance of applying an earth-air heat exchanger (EAHE) [24] in a windcatcher system or a heat transfer coil connected to a low-temperature thermal mass in the building [25].

1.2. Research problem and question

Like any natural ventilation device, windcatchers' ventilation and thermal performance largely depend on the outdoor wind and climate conditions. In the field, the wind speed and direction frequently change, unlike the stable wind conditions simulated in wind tunnels and steady-state CFD in many windcatcher studies [26]. The wind direction will not always be the same as the design wind direction, and hence, it must be considered when evaluating the ventilation technology. In a multi-opening/sided windcatcher, the supply and return airflow direction within its channels will vary as the wind direction changes and could influence the ventilation rate and the performance of the integrated low-energy or passive technologies [13,27].

As an example, as shown in Figure (1b), the efficiency of passive cooling in the conventional four-sided windcatcher will be impacted by changing wind directions or even working against it. For example, adding the cooling device in the windcatcher's windward side channel would be beneficial when the wind flow is from the same side. However, once the wind direction changes, the cooling devices (now in the leeward channel) may not be as effective, or if the wind is in the opposite direction, it will cool the exhaust air instead. Adding the cooling device in all channels will cool the supply airflow but also the exhaust airflow, which will lead to wastage. The same issue would also occur in applying the passive technology in the windcatcher with a separate inlet and outlet. For example, using a windcatcher with evaporative cooling in regions with limited water resources should consider the potential wastage of water caused by inefficient operation [28].

A windcatcher integrated evaporative cooling system had to be assisted by a fan to avoid this issue [29]. And some of the research employed a rotary windcatcher so that its inlet opening faces the wind constantly [15,30]. The same inefficiency caused by the changing wind directions would also occur when the heat recovery device was applied in the conventional windcatcher. The heat recovery in a conventional four-sided windcatcher was investigated, but the frequent switching of inlet and outlet would decrease the heat recovery efficiency [31,32]. Moreover, the supply and return area in the conventional four-sided windcatcher is not always identical, which would also decrease the heat recovery efficiency [32].

The rotary wind scoop can be used for multi-directional ventilation to supply air to the room [33,34]. However, the high capital and maintenance cost of the rotary components not only limits the size of the natural ventilation but also increases the cost of the natural ventilation. Thus, providing a low-cost substitution for the rotary wind scoop would also benefit natural ventilation applications.

1.3. Literature review and research gaps

Currently, the research about integrating windcatchers and passive cooling or heating technologies to satisfy the thermal comfort, fresh air requirements and low carbon emissions for the building sector is insufficient, and an appropriate windcatcher needs to be developed.

The impact of the changing wind direction was not always taken into account in previous research [35]. The ventilation performance of the conventional windcatcher would also be influenced by a slight change in the wind direction, and the effectiveness of passive technologies would also be affected [32,36]. Many of the studies [22,31,37,38] that evaluated the performance of passive cooling and heat recovery technologies integrated into the windcatcher focused mainly on its ability to cool or heat the incoming airflow. While its operation under varying wind directions is typically not evaluated, even though the stable performance of the system under different wind directions is important for the building [32].

In the study [20,39], an evaporative cooling system was applied in a windcatcher system to cool a greenhouse at a specific wind direction, but the impact of changing wind direction was not considered. Evaporative cooling is an effective and low-cost cooling method which has

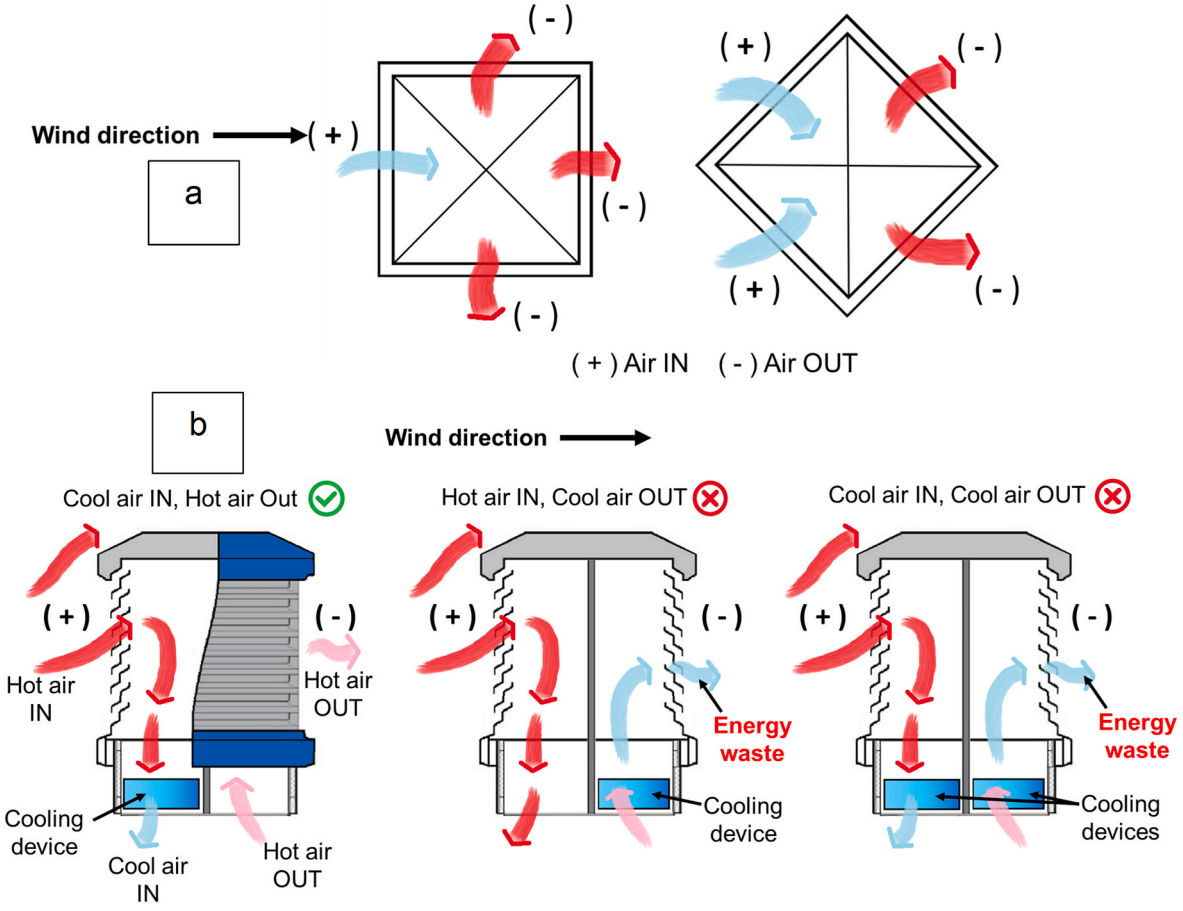

Fig. 1. Operation of (a) multi-directional windcatcher at 0° and 45° wind directions (b) conventional windcatcher with the cooling device in the windward channel, leeward channel and both channels (from left to right).

been applied in traditional windcatchers in hot and dry climates. The evaporative cooling system can also be applied in single side windcatcher assisted with solar wall to enhance the ventilation performance, but the system could not guarantee the airflow direction in the system under the changing wind direction, and the reverse flow of the solar-heated air might increase the indoor air temperature [19].

A comparison of conventional natural ventilation windcatchers is shown in Table 1. The ventilation performance and passive/low-energy technology integration were compared.

The ventilation and heat recovery performance of conventional windcatchers was already evaluated, including its integration with heat pipes [31,32,43] and thermal wheels [44]. . A case study in the UK showed that applying heat recovery in natural ventilation was effective in providing a fresh air supply with low energy consumption, but the system was sensitive to the changing wind direction [46]. Thus, multi-directional natural ventilation devices for passive/low-energy cooling and heating technology integration must be evaluated under varying wind directions.

1.4. Aim and objectives

This research aims to develop and evaluate a novel dual-channel windcatcher with inlet openings equipped with flap fins and central stack exhaust for passive or low-energy technology integration with several functions; (1) the airflow direction and ventilation rate inside the system are fixed regardless of wind direction, (2) the supply and return airflow channels are adjacent to allow heat transfer between them for example, for heat recovery, (3) the polluted air from the outlet would not contaminate the supply air, and (4) there will be no air-short circuiting. This will be achieved by the following objectives; (1) development of a scaled windcatcher prototype and evaluation of the ventilation performance in an open wind tunnel and field test experiment, (2) development of a CFD model and validation of the model with the experiment results, and (3) parametric analysis of the proposed windcatcher design including thickness, length and layout of the flap fins.

2. Experimental method

2.1. The proposed windcatcher device

The flap fin louver windcatcher was designed based on the conventional 8-side windcatcher, and the flap fins were applied at each opening to control the airflow supply based on the check valve strategy. A circular tube duct located centrally extracts the stale air out to the top of the windcatcher. The flap fin louver windcatcher, as shown in Figure (2), uses the pressure differential at the openings to control the opening and closing of the flap fin automatically. The fins are lightweight, which allows for a self-opening and -closing mechanism. As the wind blows from the windward side, the flap fin on this side will open, allowing the air to enter the windcatcher into the room below. If the pressure outside of the openings were lower than the inside, the pressure difference would force the flap fins to be attached to the windcatcher wall and block the opening, which is slightly smaller than the flap fin, to avoid air leaving the windcatcher. This effectively shuts the flap fins on the leeward side openings of the windcatcher, which are in the negative pressure region. The dynamic process of opening and closing the flap fins at different sides works similarly to a wind scoop [36] without the rotary components, which always have the opening facing the wind. The

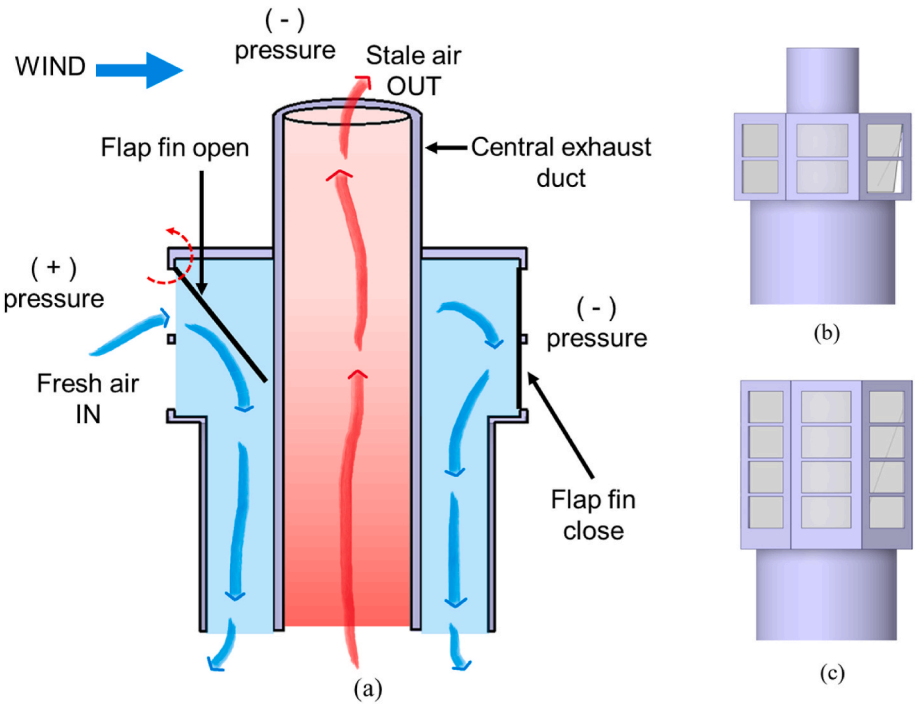

Fig. 2. Flap fin louver windcatcher concept (a) airflow diagram (b) single height model (c) double height model.

flap fin design creates a low-cost alternative to the rotary wind scoop and eliminates the rotating mechanism.

In the proposed design, the air would always enter the supply channel from the windward side openings without leaving the windcatcher channel on the leeward side as the flap fins will be closed. The stale air is extracted via the central return duct, which works as a chimney and prevents the mixing of the supply and exhaust air channels. With the combination of chimney and flap fin design, the airflow supply and exhaust direction inside the natural ventilation system will be fixed regardless of the wind direction. Hence, the adjacent concentric circular channels allow for the installation of passive or low-energy technologies to address the issues highlighted in Section 1.2.

2.2. Open wind tunnel testing and prototype

The experiment was carried out in an enclosed building in Dalian, Liaoning in China. A scaled test room with a size of 1.2 m × 1.2 m x 1.2 m cube was constructed using six 50 mm thick insulation panels and steel beam frameworks , as shown in Figure (3). The return duct of the windcatcher was extended by 0.5 m from the top of the roof to the centre of the room to increase the distance between the position of the anemometer to the start of the return duct, which stabilizes the airflow in the return duct. The airflow was transferred to a fully developed flow with a smaller centre-to-edge wind speed difference, which is ideal for the velocity measurement. Two L-shape anti-short circuit devices (ASCD) were also applied below the windcatcher to adjust the airflow direction from vertical to horizontal to achieve a better airflow distribution inside the room [47].

An open wind tunnel with an industrial fan and flow conditioners was constructed to generate stable wind around the windcatcher [36]. The fan's power was 700W, and a contraction tube was applied at the outlet, and the screen mesh, honeycomb and flow conditioner were applied before the opening to stabilize the wind [48].

The components in the open wind tunnel are shown in Figure (3). The thickness of the wire in the mesh was 0.1 mm, and the gap was about 0.3 mm. The length of the flow conditioner was about 200 mm with a diameter of 10 mm. The initial wind from the fan had a relatively low wind speed in the middle than the surroundings. A block ring was added in the middle to let the supply air pass through the middle, closing the gap between the middle and the surroundings. The wind from the wind tunnel was not perfectly uniform, but the uniformity and stability of wind speed were improved to a level sufficient for experimental measurement and result validation.

The wind speed profile from the wind tunnel was obtained by measuring the wind speed at 17 points at the open wind tunnel outlet in Figure (3). A maximum average wind speed of about 3 m/s was achieved because of the high system pressure loss caused by the screen mesh and flow conditioners. The wind speed profiles in different tests were measured for simulation validation.

The wind speed validation points are shown in Figure (3), in the vertical plane in the middle of the model. Validation point 1 was 1 cm above the bottom of the ASCD and 20 cm to the centre of the tubes. Validation point 2 was 5 cm away from the wall and 55 cm above the room's floor. The centre wind speed point was in the middle of the return duct, with a height of 5 cm above the top surface of the test room. The windcatcher frame in the prototype was constructed using a wood panel, and the flap fin was made of 0.1mm–0.25 mm polyvinyl chloride (PVC) sheets. This was selected due to the availability and strength of the materials. Fins with thicknesses lower than 0.1 mm were too soft to block the openings.

The flap fins were connected to the windcatcher frame by an adhesive film. During operation, the flap fins may become in contact with the adjacent fins (depending on the wind direction) and the internal tube; consequently, it will influence the open angle of the fins. The operation of the flap fin louver windcatcher is shown in Video (1) at 0° and 22.5° wind angles. The pressure distribution (at 2 m/s wind speed) and the open/off condition around the flap fin louver windcatcher at 0° and 22.5° wind direction, obtained from the CFD model, are presented in the result section. It should be noted that when the approach wind is from 0° wind direction, the opening and closing of the flap fins at the oblique windward facade of the windcatcher were not similar in the windcatcher models with single height and double height. The flap fins were open in the single-height model but closed in the double-height model. While the rest of the flap fins opened/closed similarly.

Supplementary video related to this article can be found at https://doi.org/10.1016/j.buildenv.2023.110429

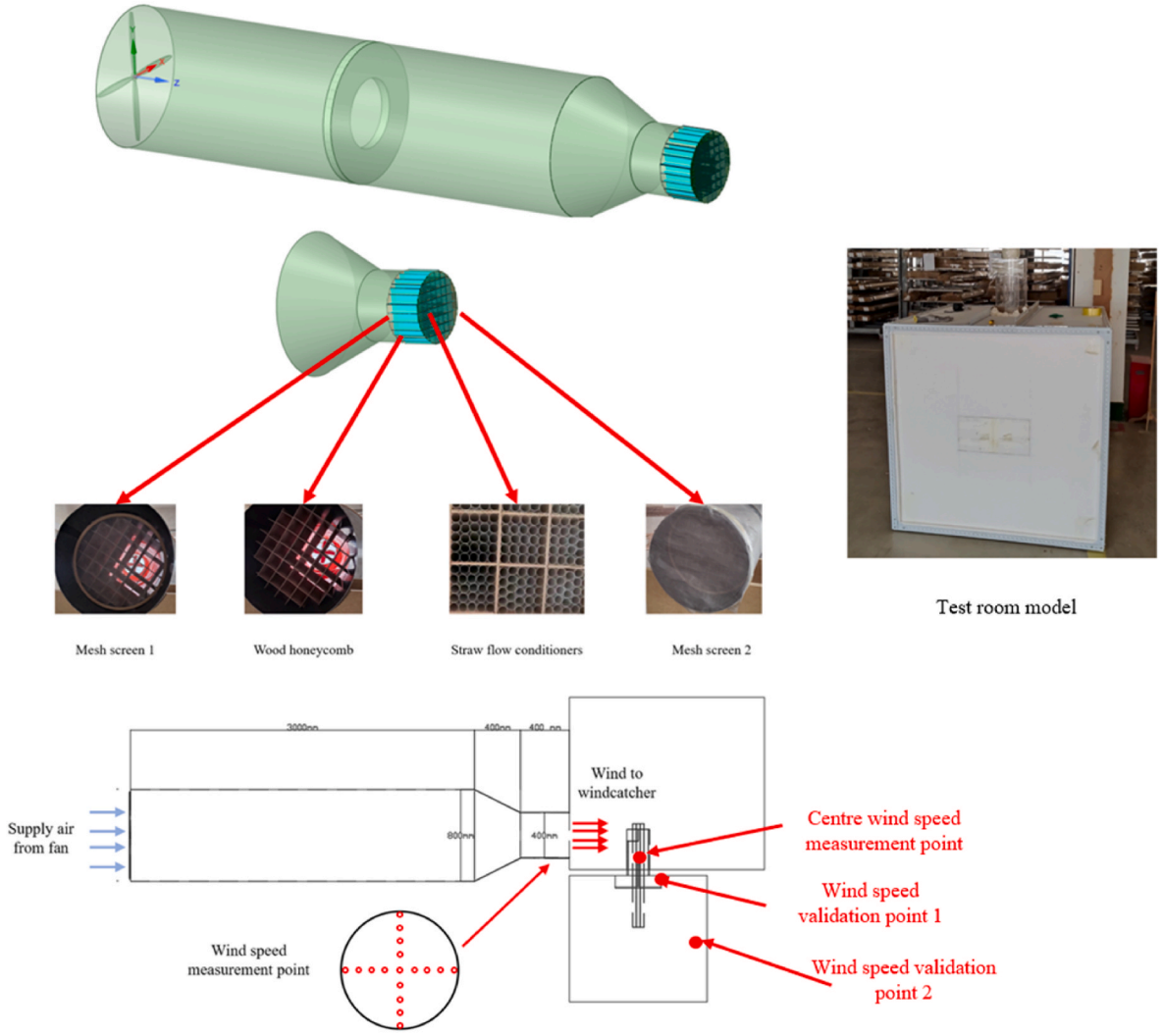

Fig. 3. Open wind tunnel specification and wind catcher setup.

The experimental model dimensions are detailed in Figures (4) and (5)(a), and this has been modelled in full scale in the numerical simulations. The inlet opening area in the double-height model was two times that of the opening area of the single-height model. The internal tube diameter was 100 mm, and the external tube was 200 mm. It should be noted that the supply and return channel areas were not balanced in the prototype, which would impact the total ventilation rate. This is because of the size of available products and the wind tunnel, which need to be optimized in future research. The windcatcher structure was made of wood, and the flap fins were made of plastic sheets. The initial design of the proposed system/concept was selected based on the ease of manufacturing and limitations of prototyping equipment.

The tracer-gas decay method using nontoxic carbon dioxide was used to measure the airtightness of the sealed test room [49]. The CO_2 concentration sensor (HTI HT2000) was used for the CO_2 concentration measurement, and the accuracy of concentration measurement at the condition below 5000 PPM was $\pm$ 50 *PPM* $\pm$ 5% of the readings. The Testo 405i hot wire hot wire anemometer was used for wind speed measurement with an accuracy of $\pm(0.1\ \mathrm{m/s}\ +\ 5\%\ \mathrm{of\ mv})$ at $0-2\mathrm{m/s}\ \pm(0.3\ \mathrm{m/s}\ +\ 5\%\ \mathrm{of\ mv})$ at $2-15\ \mathrm{m/s}$. The carbon dioxide sensor was placed in the middle of the test room.

The air change rate of the test room was calculated by the CO2 concentration change rate [50]. In the airtightness measurement, the initial CO_2 concentration was 3350 PPM, and the final CO_2 concentration was 3200 PPM. The time of air exchange was 3050s, and the outdoor CO_2 concentration was 500 PPM. The air change rate of the sealed test room was 0.0625 h^{-1}. The air leakage was 0.023L/s which was ignorable compared to the wind-forced ventilation. Thus, the test room can be treated as an airtight full airtight box in the experiment.

The ventilation rate of the windcatcher was measured by the centre wind speed in the return duct times the area of the duct and the ratio of the centre wind speed to the average wind speed in the return duct. The ratio of the centre wind speed to average wind speed was measured in the experiment, which is a function of centre wind speed. The prototype with all fins added was investigated, and the same model without the windward fins was also tested to investigate the maximum performance of the windcatcher with the windward side fins fully opened.

As the wind tunnel could only generate wind speed of up to 3 m/s and was not large enough to simulate the entire flow region, an experimental field test was conducted to investigate the performance of the windcatcher under real outdoor conditions. Two sets of tests were conducted during a typical winter period in the UK. During the tests, the outdoor wind speeds range between 0 and 8 m/s. The field study was carried out at the Jubilee campus at the University of Nottingham in the UK on a large open field. The outdoor temperature ranged between 16 and 19 °C in test 1 and 17–21 °C in test 2, and both the outdoor wind direction and speed fluctuated during the test. The operation of the prototype during variable wind conditions is shown in Video 2, and the results are detailed in Section 4.8.

The field test model and location of the model in the university are

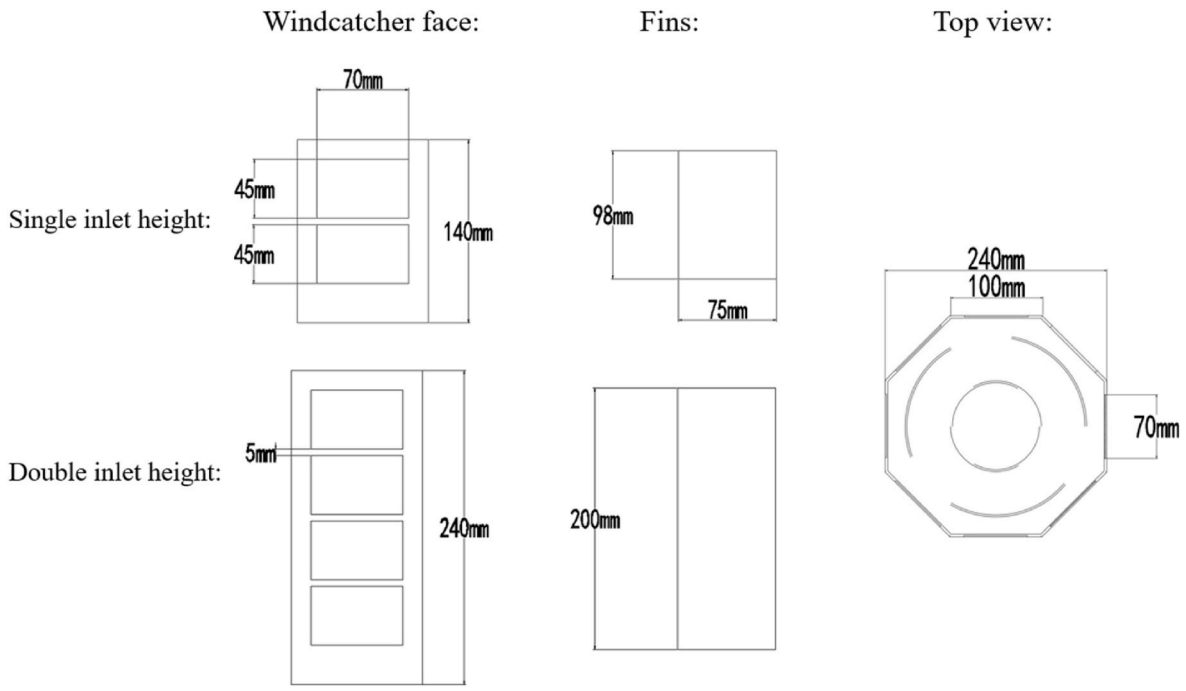

Fig. 4. Windcatcher schematic and dimensions.

shown in the Appendix. Measurements of the airflow rate were conducted using the same approach as in the wind tunnel. The measurement point of centre wind speed in the field test was about 35 cm above the test room roof. The wind speed at a 1.6 m height level, with the same height as the centre of the windcatcher, was measured using the same hot wire anemometer. The outdoor anemometer was about 5 m away from the test room model, which could rotate according to the wind. Thus, the wind speed was measured under varying wind directions.

3. CFD method

In this research, the Computational Fluid Dynamic (CFD) simulation of the proposed windcatcher was conducted by the commercial software FLUENT. The mass and momentum equations are solved for the airflow in this model. The energy governing equation was not applied as the heat transfer was not investigated in the present study to simplify the CFD simulation process. The Reynolds-averaged Navier-Stokes (RANS) model was employed with the k-epsilon, re-normalization group (RNG), turbulence model, which is capable of performing accurate simulations of airflow in similar natural ventilation systems, as highlighted in the literature including [51]. The SIMPLE algorithm was applied in the simulations [52]. In turbulent airflow simulations, the semi-implicit method is typically used, and a solver using pressure-linked equations segregated pressure-based algorithm is applied due to its robustness and computational efficiency. A second-order upwind scheme is employed to discretize all the transport equations. The governing equations for the mass (eqn. (1)), momentum (eqn. (2)), and k and epsilon (eqns. (3) and (4)) [53] are detailed below:

$$\frac{\partial \rho}{\partial t} + \nabla \times (\rho u) = 0 \tag{1}$$

where u refers to the fluid velocity vector, t is time, and ρ is density.

$$\frac{\partial \rho}{\partial t} + \nabla \times (\rho u \nabla u) = -\nabla p + \rho g + \nabla \times (u \nabla u) - \nabla \times \tau_t \tag{2}$$

Where g is a vector of gravitational acceleration, p is the pressure, τt is the divergence of the turbulence stresses, and μ is dynamic molecular viscosity.

$$\frac{\Delta}{\delta t}(\rho k) + \frac{\delta}{\delta x_i}(\rho k u_i) = \frac{\delta}{\delta x_i}\left(a_k \mu_{eff} \frac{\delta k}{\delta x_j}\right) + G_k + G_b - \rho\varepsilon - Y_M + S_k \tag{3}$$

$$\frac{\Delta}{\delta t}(\rho \varepsilon) + \frac{\delta}{\delta x_i}(\rho \varepsilon u_i) = \frac{\delta}{\delta x_j}\left(a_k \mu_{eff} \frac{\delta \varepsilon}{\delta x_j}\right) + C_{1\varepsilon}\frac{\varepsilon}{k}(G_k + C_{3\varepsilon}G_b) - C_{2\varepsilon}\rho\frac{\varepsilon^2}{k} - R_\varepsilon + S_\varepsilon \tag{4}$$

where *Gb* and *Gk* represent the generation of turbulence kinetic energy due to buoyancy and mean velocity gradients. Y_M defines the overall dissipation rate. α_k and α_ε are the inverse effective Prandtl numbers for *k* and ε. S_k and S_ε are user-defined source terms.

It should be noted that the validation CFD model was based on the open wind tunnel experiment. The CFD settings are detailed in Table 2. The inlet wind speed and profile were based on the open wind tunnel experiment. The pressure outlet was set to atmospheric or 0Pa. Default values were set for the turbulence kinetic energy. The convergence criteria were set based on the values in Table 2.

The supply and return duct section areas were not perfectly balanced, which resulted in a higher airflow velocity in the return duct and a higher pressure loss than in balanced supply and return channels. As shown in Figure (5)(a), the return duct was extended into the room, by 350 mm, to increase the distance between the wind speed measurement point and the inlet of the return duct to reduce the airflow velocity difference between the middle and the side. This extension was necessary for better experiment measurement accuracy with a lower wind speed difference between the middle and edge, as the airflow in the return duct got more uniform after entering the return duct for a longer distance. However, the extension is not necessary for the real application, which takes the space in the room and increases the system pressure loss.

In the CFD simulation model in Figure (5), the full wind tunnel geometry was not included in the simulation, and instead, a circular inlet was modelled to simulate the outlet of the open wind tunnel. Only the region around the windcatcher and inside the room was simulated in the CFD model to simplify the simulation. By using the wind speed profile at the outlet of the open wind tunnel measured from the experiment, the inlet wind speed profile was applied in the simulation first to validate the CFD simulation model.

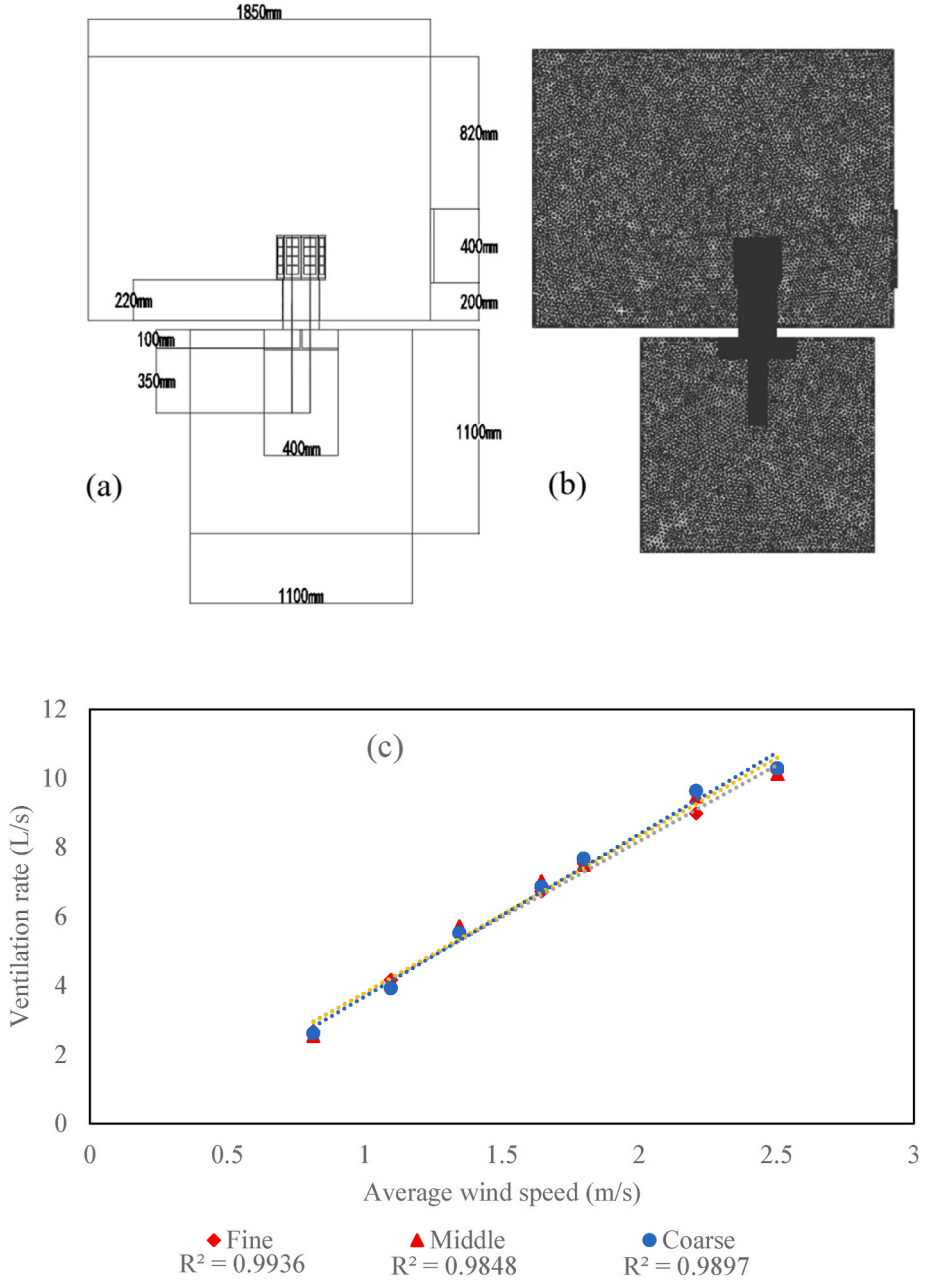

Fig. 5. (a) CFD simulation domain and dimensions in mm (b) mesh of the simulation model (c) mesh independence analysis result.

Table 1
Comparison of conventional windcatchers for natural ventilation.

Windcatcher type	Sensitivity to wind direction	Passive or low-energy technology integration	Advantages	Disadvantages
Single-sided windcatcher/ Wind tower [15]	High	• Earth-air heat exchanger [37] • Evaporative cooling [38]	Low cost	Sensitive to wind directions
Two-sided windcatcher [40]	High	• Evaporative cooling spray or cloth [22]	High ventilation rate at design wind direction	Sensitive to wind directions
Four-sided windcatcher [41, 42]	Middle	• Heat pipe for cooling and heat recovery [31,32,43] • Thermal wheel [44]	Good ventilation performance Passive technologies applied	Passive technologies are sensitive to wind direction
Eight-sided or more openings windcatcher [45]	Low	None	Insensitive to wind direction	Low ventilation rate No appropriate passive technologies
Flap fin louver windcatcher	None	• Solar heating • Heat pipe heat recovery	Insensitive to wind direction Passive technologies and heat recovery applied Low cost	Lower peak ventilation rate than traditional windcatcher Need further investigation for commercial use

Table 2
CFD settings and boundary conditions.

Term	Value and settings
Inlet	
Velocity (m/s)	0-3 (wind profile based on the wind tunnel)
Initial Gauge Pressure (Pa)	0
Turbulence Model	K-epsilon RNG
Turbulence Kinetic Energy (m^2/s^2)	1
Outlet	
Gauge Pressure (Pa)	0 (atmospheric)
Wall (domain and windcatcher)	
Shear Condition	No slip
Roughness Model	Standard
Roughness Height	0
Roughness Constant	0.5
Converged residuals	
Continuity/k/Epsilon	0.001
X/Y/Z velocity	0.0001

The number of elements for the fine, medium and coarse mesh in the independence analysis were 3.2 million, 1.2 million and 0.3 million, respectively. The double height with single fin model was selected for the mesh independence analysis, and the results are shown in Figure (5)(c). The ventilation rates predicted by the model with different mesh sizes were compared for the mesh independence analysis to support the model verification. In the model with different mesh qualities, the maximum ventilation rate gap reached 0.5 L/s, but most of the results were identical, and the trend lines of the ventilation rate to the outdoor wind speed matched well. Although the R^2 values of the simulation results achieved from the three mesh qualities were not identical, all the R^2 values were higher than 0.98, which provided a linear relationship between wind speed and ventilation rate. Thus, for the ventilation rate evaluation in this research, the simulation model was independent of the mesh quality. The fine mesh quality with about 3.2 million mesh elements, in Figure (5)(b), was selected for the final simulation validation, with the highest R^2 value in the research.

A conventional 8-sided windcatcher with similar geometry to this research was selected for ventilation performance comparison as the ventilation rate of the 8-sided windcatcher was almost independent of the wind direction. A fixed 8-sided windcatcher model with the same opening size as the flap fin louver windcatcher in this research was made. The simulation settings and outdoor wind speeds in the 8-sided windcatcher simulation were identical to the previous validation model.

4. Results

4.1. Experimental validation

In Figure (6a), the y-axis is the distance between the wind speed measurement point and the centre of the wind tunnel, and the x-axis is the wind speed. As shown in Figure (6a), the wind speed profile is a quadratic function of the distance to the centre of the wind tunnel outlet. The velocity in the middle was slightly lower than the surroundings, and the wind speed on the edges was lower because of wall friction. With the increase in average wind speed, the gap between the maximum and minimum wind speeds would also increase. The equation of the wind speed profile is detailed in the Appendix. The error range of the wind speed was determined by the percentage calculated from the hotwire anemometer sensors' accuracy based on the calibration data.

The CFD model validation was achieved by different methods, including the wind speed profile in the return duct in Figure (6b) and the wind speed in three validation points in Figure (7). The wind speed profile in the return duct in the CFD simulation and experiment could match each other very well, as shown in Figure (6b). In Figure (6b), the y-axis is the distance between the wind speed measure point and the centre of the return duct, and the x-axis is the wind speed. Thus, the relationship between the centre wind velocity to the average wind velocity in the return duct was calculated, and the ventilation rate can be calculated. The correlation factor of average velocity to centre velocity was a function of the centre wind speed, as the wind speed would have an impact on the Reynolds number and the development of airflow inside the tube.

The approximation formula of the velocity in this experiment is shown in Equation (5):

$$\overline{V} = (0.9627 - 0.022 \times V_c) \times V_c \tag{5}$$

where $\overline{V}$ is the average airflow velocity in the return duct in m/s;

V_c is the airflow velocity in the centre of the return duct in m/s.

The ventilation rate was calculated by Equation (6):

$$Q = \overline{V} \times A = (0.9627 - 0.022 \times V_c) \times V_c \times A = -0.00017 \times V_c^2 + 0.00756 \times V_c \tag{6}$$

where Q is the ventilation rate in L/s,

A is the section area of the return duct in m^2.

Wind speed under different wind directions was also compared. The difference between the wind speed measurement and CFD model result was negligible.

The ventilation performance of the model without the windward side fins was also investigated and validated. This will be compared with the

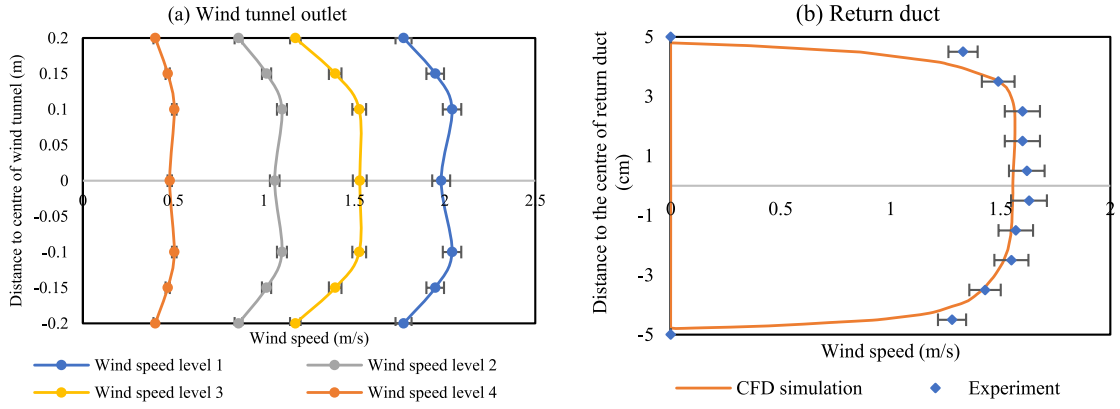

Fig. 6. Wind speed profile in the (a) open wind tunnel outlet and (b) return duct, comparing CFD results against experimental measurements.

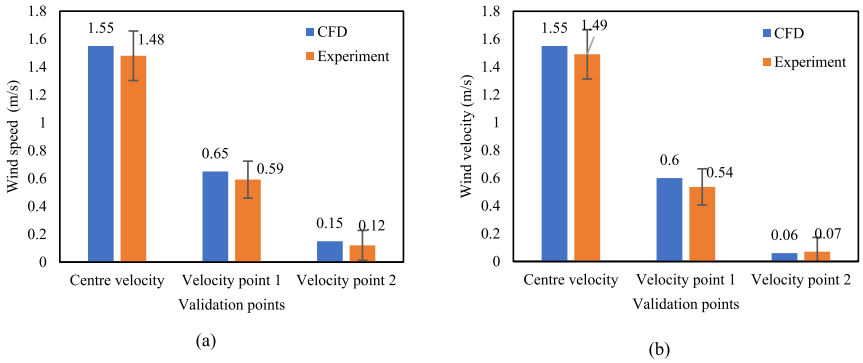

Fig. 7. Wind speed validation results for (a) wind direction 0° and (b) wind direction 22.5°.

model with the windward side fins to evaluate the impact of the mass and the geometry of the fin. As shown in Figure (8), a linear relationship between ventilation rate and environment wind speed was achieved. The average difference between the ventilation rate in the experiment and simulation was 0.25L/s with an average error of 4.1% in the condition with wind from the edge direction (22.5° wind). And the average difference between the ventilation rate in the experiment and simulation was 0.23L/s with an average error of 5.6% in the condition with wind from the face direction (0° wind). The trendlines of the simulation and experiment results were almost overlapped, and the error was within the accuracy range of the anemometer.

The ventilation rate of the windcatcher model with double height and single long fins was also validated. The trendline of the ventilation rate in the model with all the fins differed from the model without the windward fins. As shown in Figure (9), a linear relationship was achieved after 1 m/s wind speed. The poor ventilation rate of the flap fin louver windcatcher was caused by the energy loss on pushing up the plastic sheet. Under the low outdoor wind speed conditions, the wind was not able to push the fin up, and the small opening angle of the fin resulted in a blockage of airflow. The average difference between the ventilation rate in the experiment and simulation was 0.16L/s with an average error of 4.5% in the condition with wind from the edge direction (22.5° wind). And the average difference between the ventilation rate in the experiment and simulation was 0.09L/s with an average error of 2.3% in the condition with wind from the face direction (0° wind). The trendlines of the simulation and experiment results almost overlapped, and the error was within the accuracy range of the anemometer.

The present study involved the measurement of the average wind speed and ventilation rate in a controlled environment, where the wind speed was held constant. Although the supplied wind was stabilized

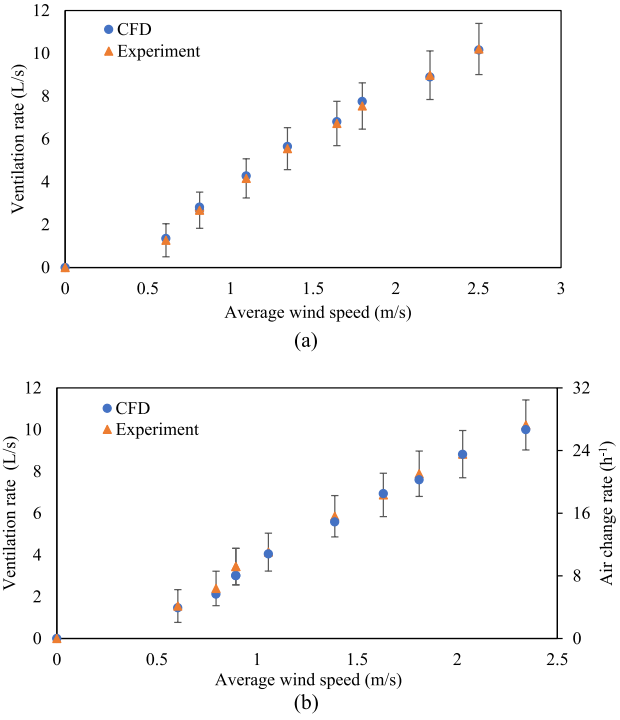

Fig. 9. Ventilation rate validation of the windcatcher with all fins at (a) 0° wind and (b) 22.5° wind.

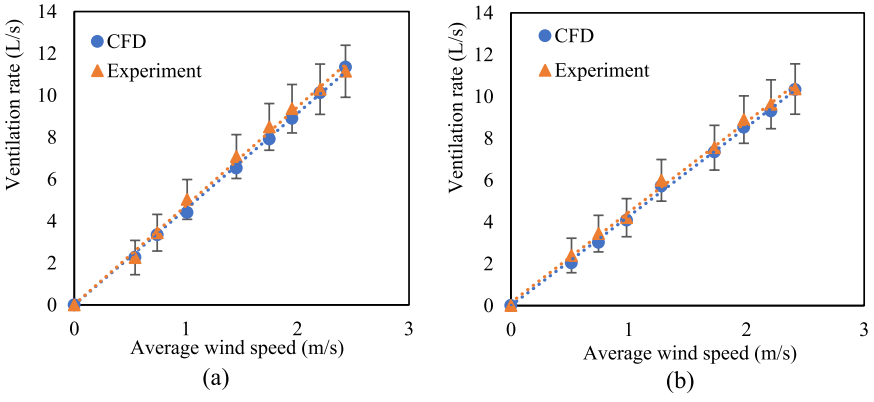

Fig. 8. Validation of the ventilation rate for the windcatcher without the windward side fins at (a) 0° wind (b) 22.5° wind.

using a wind tunnel, the plastic sheet still exhibited fluctuations within a narrow range around the neutral position.

To validate the computational fluid dynamics (CFD) model employed in this research, we conducted a comparison of wind speed profiles at various points in the return duct and evaluated the relationship between ventilation rate and environment wind speed. Our analysis revealed that the CFD simulation results were sound and met the standards required for this study.

4.2. Airflow distribution and ventilation performance

The airflow velocity contour is shown in Figure (10). Based on the contour plot, the airflow was observed to enter the inlet boundary wall on the right side, and then it split into two streams. A portion of the airflow entered the flap fin louver wind catcher, while the other portion exited through the pressure outlet. The contour plot also revealed the presence of air recirculation on the leeward side of the windcatcher. Upon entering the windcatcher, the airflow was redirected downwards by the front flap fin and channelled through the L-shaped anti-short circuit device, which facilitated the supply of air into the room. As the airflow moved through the side walls, it decelerated and eventually reached the room floor. Subsequently, the airflow was directed towards the centre of the floor and flowed upwards towards the central chimney, which extracted the air out of the space. Despite the low velocity of air inside the room, the airflow was found to be well-circulated, and fresh air was supplied to the level of occupants. However, it is worth noting that further design optimization is necessary to enhance the airflow speed in the room.

From the top view, Figure (11)(a) shows the open/close condition of the flap fins and pressure distribution (at 2 m/s outdoor wind speed) around the flap fin louver windcatcher when the wind direction is at 0° and 22.5°. The air striking the windward surface exerted a positive pressure on the inlet face, which opened the front flap fins and forced air through windcatcher openings. Concurrently, while the windward surface experiences this positive pressure, the external pressure surrounding the leeward side fins remains predominantly negative. This pressure disparity between the internal and external environments of the fin prompts its adherence to the windcatcher wall, effectively closing the aperture and regulating the airflow within the structure.

As shown in Figure (11), the pressure dynamics within the interior environment are critical in facilitating effective airflow. The pressure at the inlet exceeds that of the room, thereby inducing the ingress of air into the enclosed space. Conversely, the pressure at the outlet is lower than that of the room, resulting in the extraction of air via the chimney. The presence of a sharp edge at the front of the outlet opening contributes to the formation of a low-pressure zone above the windcatcher. Consequently, situating the opening at the apex of the windcatcher can augment the ventilation rate through the enhancement of negative pressure surrounding the outlet. The successful implementation of replacement ventilation is contingent upon the strategic manipulation of pressure differentials among the inlet, room, and outlet, which culminates in the establishment of an optimal airflow direction.

4.3. Impact of the thickness of flap fins

The influence of the fin mass variations was examined within the context of a single-height windcatcher model. The designated fin measurements included a length of 98 mm and a width of 78 mm. The fin with a thickness of 0.1 mm had a mass of 0.91g per individual fin, whereas the 0.25 mm thick fin had a mass of 2.19g per fin. According to the data presented in Fig. 12, the ventilation rate of the model employing a 0.1 mm fin exhibited a linear correlation with the outdoor wind speed beyond a threshold of 0.5 m/s. Furthermore, the disparity in ventilation rate between models equipped with windward fins and those without diminished as the environmental wind speed increased. A similar trend was observed in the model utilizing a 0.25 mm fin upon reaching an environmental wind speed of 1.5 m/s. Notably, a reduction in the fin's mass led to an increase in the ventilation rate at identical

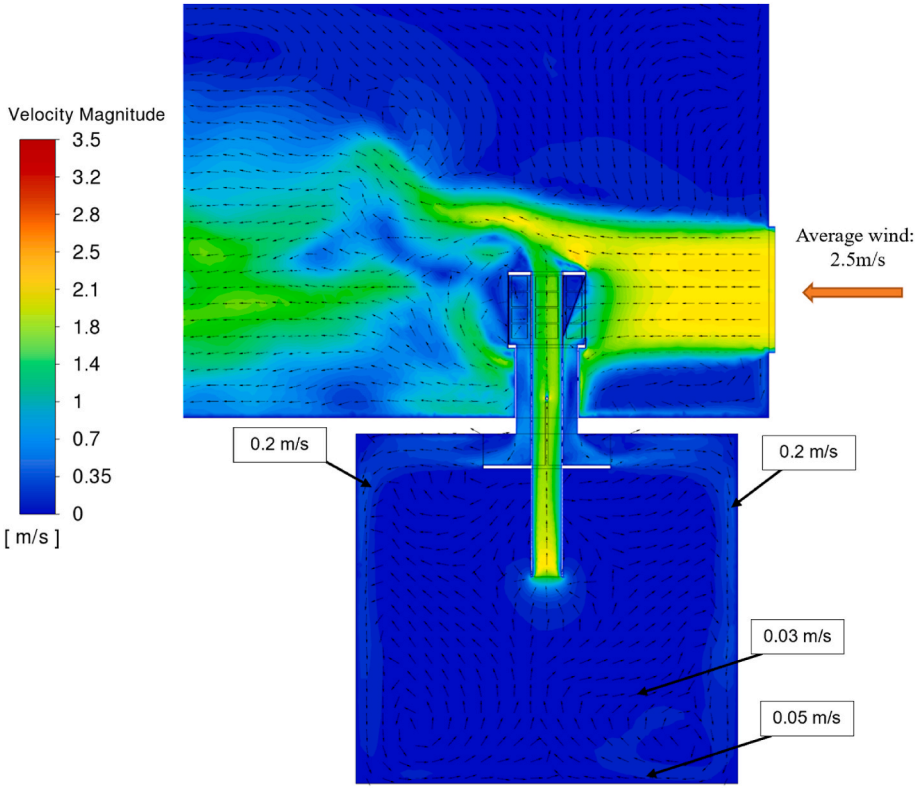

Fig. 10. Wind speed contour and vector (in-plane) in the model.

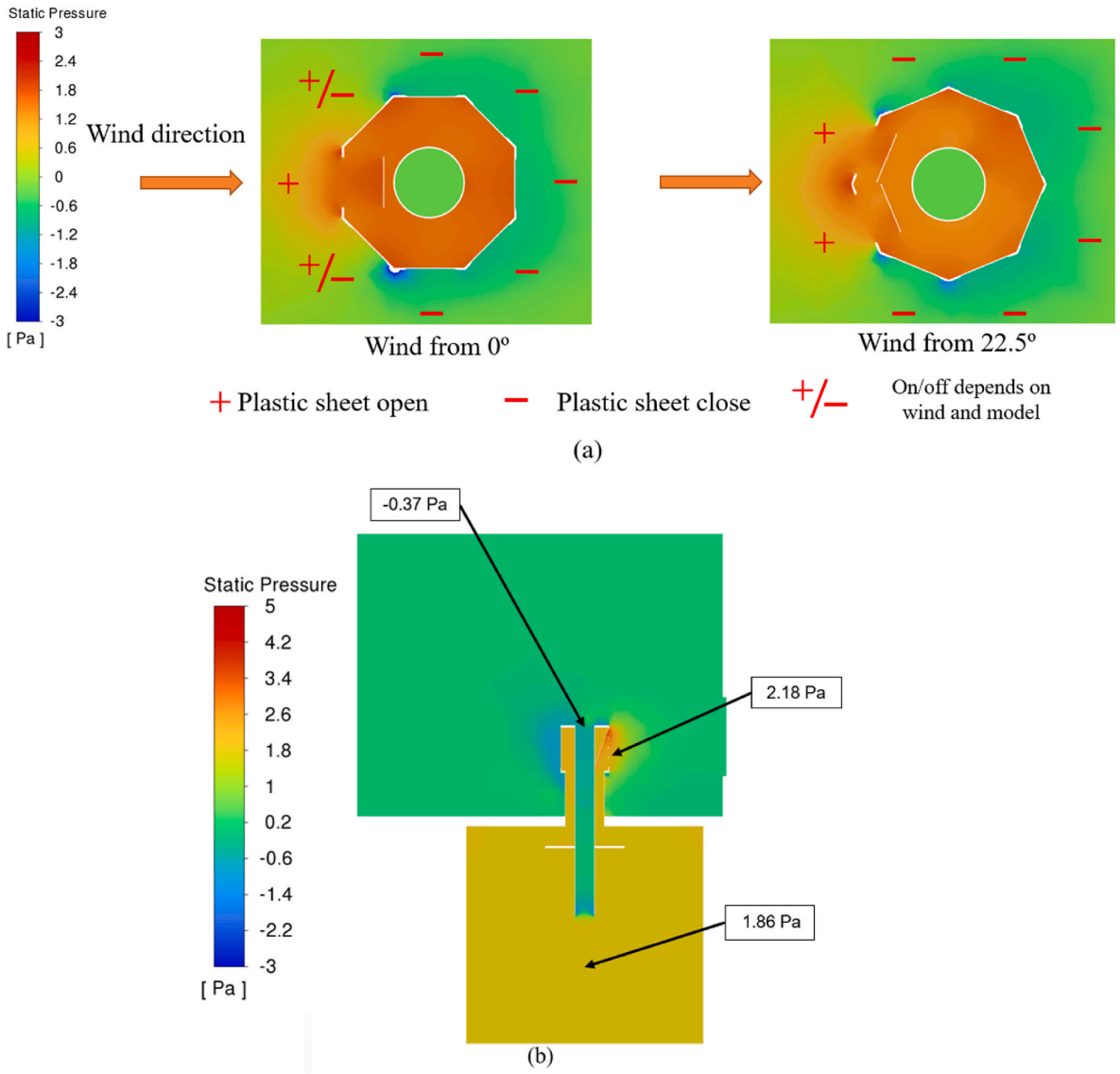

Fig. 11. (a) Open and close status of flap fins at each opening at 0° and 22.5° wind direction and (b) static pressure distribution in and around the windcatcher and room model.

wind speeds. This modification also lowered the critical environmental wind speed from 1.5 m/s to 0.5 m/s. Therefore, it can be deduced that the reduction in the fin's mass contributes to enhancing the overall ventilation performance.

The analysis also incorporated a comparative study of the ventilation rate for the model without the windward fin to discern the impact of the fins. In the context of a fixed windcatcher without flap fins on the windward side (a fixed windcatcher), the ventilation rate exhibited a linear relationship with the outdoor wind speed. The ventilation performance of the flap fin windcatcher exhibited a gradual increase prior to reaching a critical environmental wind speed of approximately 1 m/s. This trend can be attributed to the fact that the wind's kinetic energy at this stage was insufficient to allow the fin to open. Consequently, the fin maintained a predominantly closed position. As the outdoor wind speed increased, the discrepancy in ventilation rate between the models utilizing 0.25 mm and 0.1 mm fins, as well as between the model with a 0.1 mm fin and the model without a windward fin, decreased. The findings suggest that an increase in outdoor wind speed lessens the influence of the windward fin on the ventilation performance.

4.4. Impact of length of flap fins

Figure (13) presents an analysis where the doubling of the height not only increases the length of the plastic sheet but also expands the size of the opening, thereby enhancing wind capture. Thus, an in-depth investigation was conducted on the model with a double inlet height and two plastic sheets, to facilitate a comparative study with the models incorporating a double inlet height with one plastic sheet and a single inlet height. Upon retaining a constant fin length, the increased of height yielded a higher ventilation rate compared to the single-height model. Moreover, the substitution of two shorter fins with a longer one led to an increase in the ventilation rate. Upon integrating a single elongated fin in lieu of two distinct fins within the double-height model, the disparity in the ventilation rate between models with and without a front fin was reduced.

4.5. Impact of outdoor wind directions

As demonstrated in Figure (14), an analysis of wind direction's impact on ventilation rate reveals that in the single-height model, the wind emanating directly from the windcatcher face direction,

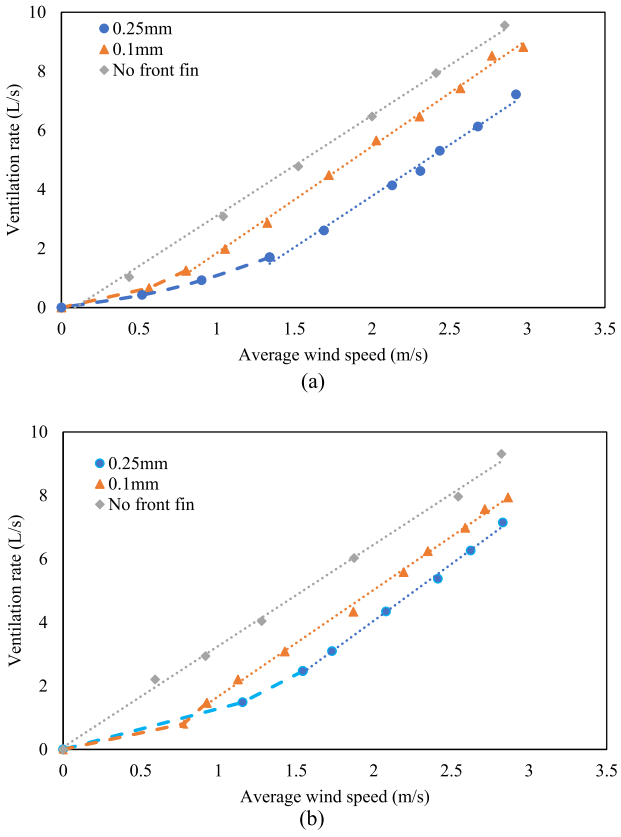

Fig. 12. Comparison of the mass of the flap fins (a) 0° wind (b) 22.5° wind.

designated as 0° wind, yielded a marginally higher ventilation rate compared to the wind originating from the edge direction, denoted as 22.5° wind. However, this discrepancy was negligible when compared with the performance of conventional multiple opening windcatchers. In the context of the double-height model, the influence of wind direction was virtually non-existent, and the ventilation rates under both conditions were largely equivalent.

4.6. Impact of the layout of flap fins

Figure (15) presents the comparative analysis between horizontally and vertically hinged fin models conducted in the present study. A noteworthy advantage of the horizontally hinged fin model lies in its reduced dependency on the fin's mass and the near elimination of gravity's impact. Conversely, in the vertically hinged fin model, gravitational force compels the closure of the plastic sheet, thereby restricting the opening angle under conditions of low wind speed. Despite these observations, the ventilation performance of the model equipped with a long, horizontally hinged fin remains inferior to that of the vertically hinged fin model. However, it would be precipitate to conclude that the vertically hinged fin model outperforms the horizontally hinged model solely based on these results. This might be due to the longer length of the vertically hinged fin, which generates higher torque to open the fin. In the current prototype, efforts have been made to minimize the fin's mass, with the fin being attached to the windcatcher wall by tap to further minimize the impact of fin mass. Future iterations of the proposed windcatcher system may necessitate modifications in the fin's material, connection, and size to ensure reliable long-term operation, thus underscoring the continued relevance of testing horizontally hinged fins. Additionally, in the horizontally hinged fin model, the fins do not obstruct each other, thus enabling the utilization of larger opening sizes.

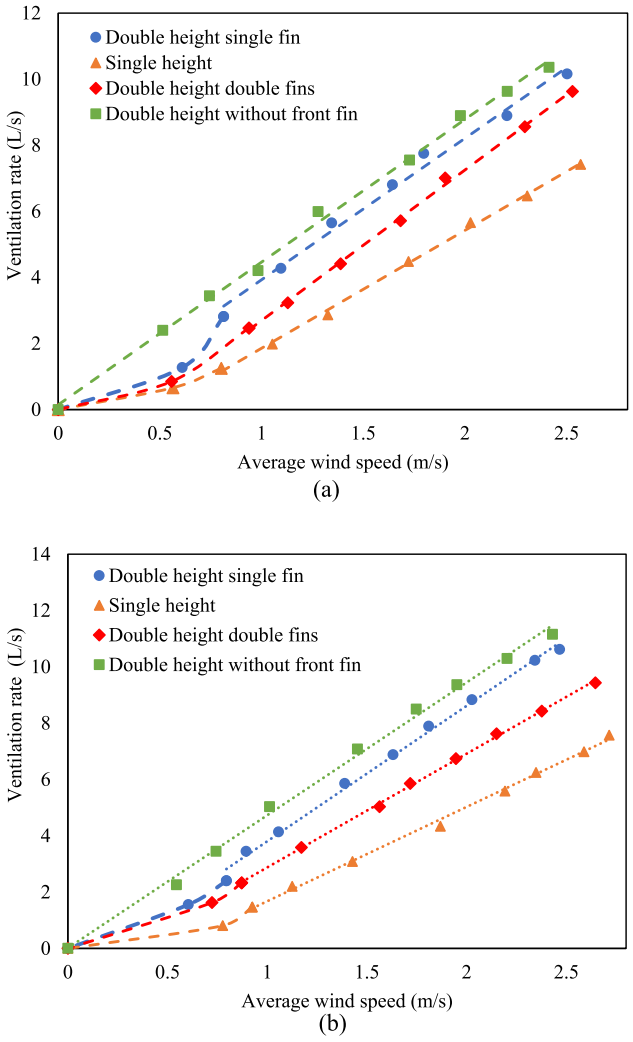

Fig. 13. Comparison of the length of the flap fins (a) 0° wind direction (b) 22.5° wind direction.

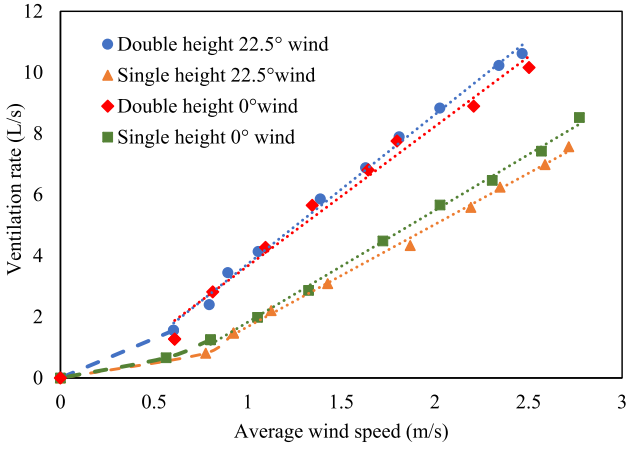

Fig. 14. Comparison of ventilation rate under different wind directions.

4.7. Comparison with a standard 8-sided windcatcher

As depicted in Fig. (16a), a traditional 8-sided windcatcher serves as the point of comparison, with the resultant comparative data presented

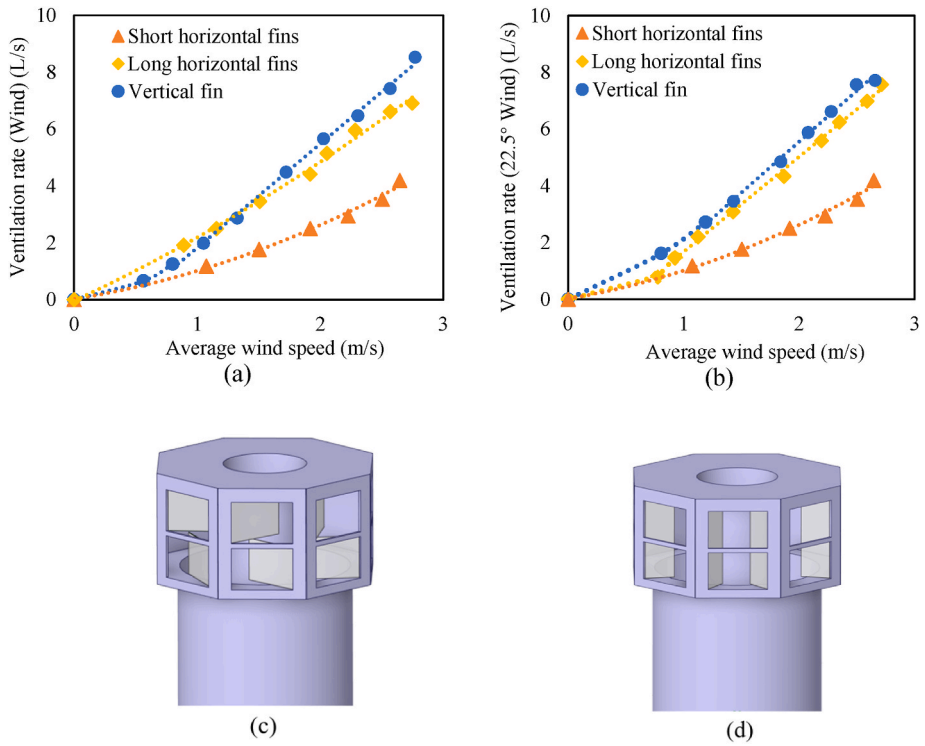

Fig. 15. Horizontally hinged fin models and ventilation performance comparison (a) 0° wind (b) 22.5° wind (c) long horizontally hinged fins model (d) short horizontally hinged fins model.

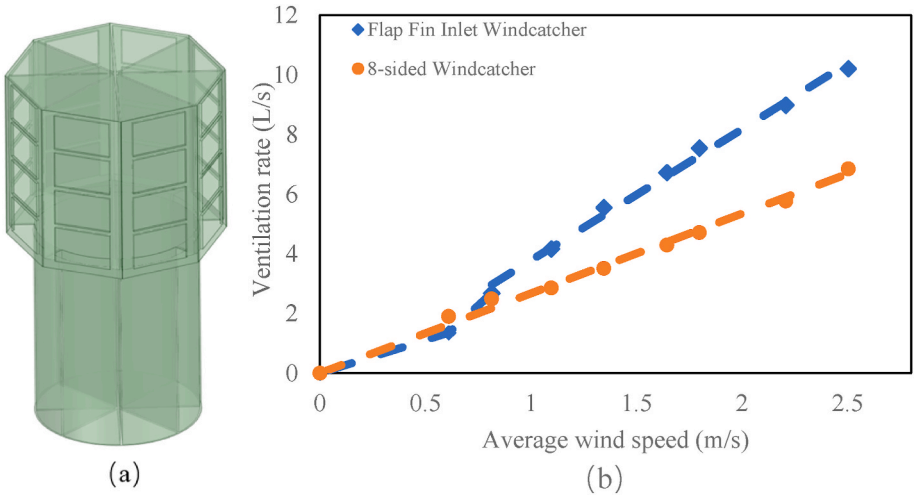

Fig. 16. Comparison of the ventilation rate between the (a) traditional 8-sided windcatcher and (b) flap fin louver windcatcher at 0° wind.

in Fig. (16b). Upon exceeding a wind speed of 1 m/s, the ventilation performance of the flap fin louver windcatcher surpasses that of the 8-sided windcatcher. Within the 8-sided windcatcher, a majority of the air is channeled into the room via two or three front openings. This results in an elevated wind speed within the supply channels and a higher total pressure loss relative to a windcatcher configured with balanced supply and return channel areas. Furthermore, the low-pressure zone located at the apex of the flap fin louver windcatcher exhibits a more substantial negative pressure compared to the rear and sides of the 8-sided windcatcher. This facilitates the extraction of a greater volume of air from the outlet openings. Despite the influence of the flap fin on the ventilation performance of the flap fin louver windcatcher, its ventilation performance remains superior to the 8-sided windcatcher. As illustrated in Fig. 11, the presence of a sharp edge at the front of the windcatcher engenders a relatively lower pressure zone above the windcatcher. Consequently, a larger negative pressure is generated at the outlet of the flap fin louver windcatcher, promoting more effective air extraction from the room. This mechanism contributes to a ventilation process that is more efficient than that of a traditional 8-sided windcatcher.

4.8. Results of the field study experiment

Figure (17) presents an empirical examination that reveals a robust linear relationship between the average ventilation rate per minute and the outdoor wind speed, notwithstanding the changing wind conditions during the test. This examination facilitated a comparative analysis of results from two field tests conducted under high and low outdoor wind

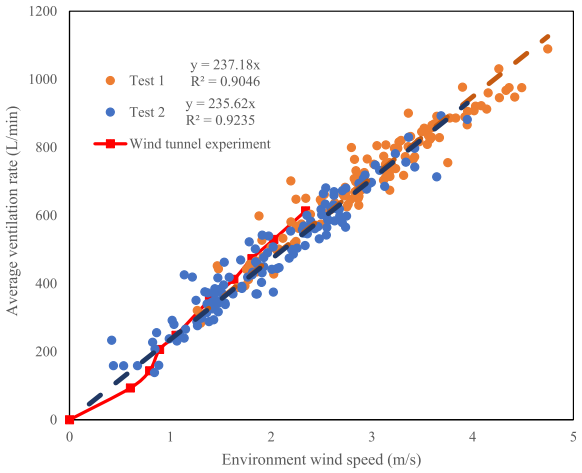

Fig. 17. Field test results of average ventilation rate against the open wind tunnel experimental results.

speeds. Remarkably, the trend lines from both tests converged closely, as indicated by an R^2 value exceeding 0.99. These findings provide empirical validation of the stable performance of the flap fin louver windcatcher across varying environmental wind speeds and directions. However, due to differences in wind speed generated by the wind tunnel—owing to factors such as the atmospheric boundary layer profile and the edges of the test room—it was infeasible to replicate precisely the performance in the field study. Consequently, the average ventilation rate in the field test was marginally lower than that in the experimental setup. Nevertheless, the field test demonstrated a ventilation performance comparable to that observed in the open wind tunnel test. Under conditions of low environmental wind, the experimental ventilation rate slightly exceeded the findings from the field study. The ventilation rates recorded per second are also furnished in the Appendix.

Video (2) provides a visual demonstration of the windcatcher's operation under varying wind directions. Initially, the wind emanates from the left-hand side, which triggers the opening of the fins on the left. Subsequent alteration of the wind direction from the left-hand side to the right-hand side elicits an immediate response: the fins on the left close swiftly, while the fins on the right open simultaneously. This video evidence underscores the capacity of the windcatcher to operate effectively under changing wind directions, while also exhibiting a rapid response to shifts in wind direction.

Supplementary video related to this article can be found at https://doi.org/10.1016/j.buildenv.2023.110429

5. Discussions and limitations of research

In this study, the dimensions of the windcatcher for the experiment and simulations were decided based on the size of the experimental room, the size of the experimental open wind tunnel and the available experimental space. The size of the wind tunnel was limited by the space of the experiment, uniform wind requirement and the wind speed demand which further limited the size of the windcatcher. Since we aimed to validate the numerical model with the experiment, we ensured that we replicated the same geometry in the numerical modelling work. This will ensure that a fair comparison can be made between the two approaches. In practice, the dimensions of the windcatcher can be determined based on the area/volume and ventilation demand of the building, similar to our earlier works [54,55]. The current system is not sized based on an actual building or installation, as the current research is still in the initial stages of development. Future works can focus on evaluating how the flow rate scale on the dimensions of the windcatcher.

Regarding the materials of the windcatcher employed in the experiment, the frame in the prototype was the wood panel and the flap fin was made of 0.1mm–0.25 mm polyvinyl chloride. Clearly, this prototype was not designed for actual or real building installations and more work is required to develop a close-to-market prototype, which can withstand various weather conditions. The selected materials in the experiment were due to various factors including the prototyping capabilities and cost restrictions.

The ventilation performance of the windcatcher was strongly affected by the opening angle of the fins, especially at low wind speed conditions. The connection at the joint and the mass of the fin had a large impact on the fin's open angle. In the current prototype, the fin mass was minimized by using a light and thin PVC material, but other materials like metal foil/film could be considered. Balancing the mass of the fin to reduce the impact of fin mass and decrease the friction at the hinge joint is necessary for optimizing performance.

The initial results showed that the adjacent fins would be in contact with each other, limiting the open angle of fins in specific wind directions, and this issue resulted in the different fin open angles at the wind from edge condition (22.5° wind). The blocking effect limited the performance of the flap fin louver windcatcher when the flap fin design was applied in the traditional four-side windcatcher. Thus, the final windcatcher in this research had an eight-sided design. In future research, the face number of the flap fin louver windcatcher can be further increased, and the issue can be avoided by a larger angle between the adjacent windcatcher face. The opening size could also be smaller than the face of the windcatcher to avoid the adjacent fins blocking each other.

Furthermore, to increase the opening angle of the flap fin, a necessary gap between the external to internal duct has to be provided in the prototype. With the limitation of the total windcatcher area and the gap, the current section area of the supply duct and return duct was not balanced and the ventilation rate was not maximized. Further optimization of the supply-to-return area ratio needs to be applied in the later application to improve ventilation performance.

An open exhaust or chimney was used in this windcatcher design. However, an open chimney without any protection was not practical for real applications because of the entry of rain, snow and insects. The exhaust outlet needs to be integrated with a chimney cap or cowl to protect the outlet from the rain or be combined with a rotary turbine ventilator or a flap fin outlet design.

Finally, the current research tests the ventilation performance of the flap windcatcher and the windcatcher integrated with the passive technologies needs to be investigated further, including solar heating using the windcatcher tube or roof, evaporate cooling, heat pipe heat recovery, earth-air heat exchanger or phase change materials. The internal duct could be further extended above the top of the windcatcher and painted black to generate a solar chimney effect and increase the ventilation rate. The water spray system could also be placed in the supply channel to cool the supply air. The heat recovery can be achieved with metal fins, tubes or heat pipes between the supply and return channels as the channels were adjacent and the airflow direction would not be changed during the operation.

6. Conclusion and future works

A flap fin louver windcatcher design was proposed with the function of; (1) the airflow direction and ventilation rate inside the system are fixed regardless of wind direction, (2) the supply and return airflow channels are adjacent to allow heat transfer between them for example, for heat recovery, (3) the polluted air from the outlet would not contaminate the supply air, and (4) there will be no air-short circuiting. This windcatcher addresses the issue of the incorporation of passive/low-energy heating and cooling technologies in conventional windcatchers. With the fixed and adjacent supply and return channels not affected by the changing wind direction, passive/low-energy technologies can be applied in this windcatcher, such as solar heating and heat

transfer devices.

An open wind tunnel and a test room were built to test the flap fin louver windcatcher. The wind tunnel could provide a stable wind supply to the windcatcher with an average wind speed between 0 and 3 m/s, and the test room was airtight with an airtightness of 0.0625 h^{-1}, evaluated by the tracer-gas decay method using carbon dioxide. The ventilation performance of the flap fin louver windcatcher under different environments and wind speed was measured in this research, and the impact of each component was also compared, including the length, weight and open direction of the fins. Increasing the length of the fin and decreasing the mass of the fin could improve the ventilation rate effectively. The ventilation rate decrease caused by the fin could be decreased to an ignorable level at high wind speed conditions so the flap fin louver windcatcher could provide a stable fresh air supply in a high but turbulent wind environment.

The validation of the CFD model and experiment model was carried out in this research by comparing the wind speeds at different locations in the model and the ventilation rate at different outdoor environment wind speeds and wind directions. The mesh independence analysis was conducted, and the ventilation rate results showed that it was independent of the mesh quality. The average ventilation rate difference was within 0.09L/s-0.25L/s in different models, and the average error percentage was within 2.3%–5.6%. The ventilation performance of the windcatcher was also verified in the field tests with varying wind speeds and wind directions. The relationship between the average ventilation rate and environment wind speed in the field test was similar to the results in the experiment and the ventilation rate of the windcatcher was independent of the environment wind directions.

The ventilation rate of the flap fin louver windcatcher was higher than the traditional 8-sided windcatcher with the same opening size under an environment wind speed higher than 1 m/s, because of a higher pressure difference between the inlet and the outlet and a lower system pressure loss.

The cost of the windcatcher is lower than the current products with a similar function, such as the rotary wind scoop. The impact of the mass and geometry of the fin was investigated to optimize the ventilation performance in the experiment and the impact of flap fins on the ventilation rate was minimized. The ventilation performance of placing the fins horizontally was also investigated in the experiment. The current scaled experiment model with a diameter of 20 cm could provide about 10L/s fresh air supply at 2 m/s environment wind speed with an air change rate over 27 h^{-1}. The full-scale model investigation and ventilation rate optimization need to be tested in further research.

In future research, the geometry of the windcatcher needs to be further optimized, such as adjusting the surface of the windcatcher faces and using deformable fins. And passive heating, cooling, and energy recovery technologies need to be applied in the fixed supply duct. Passive heating using solar thermal and passive cooling using evaporative or absorption cooling should be investigated by experiment and field study, and the possible passive dehumidification method should be evaluated. The ventilation performance of a larger windcatcher with an appropriate flap fin design should be evaluated in a larger wind tunnel in further research. The flap fin design was applied in this research to create a controlled inlet, and a similar flap fin design could also be used in an extract chimney as an outlet with reversed fin direction, which can avoid the reverse flow of pollutants.

CRediT authorship contribution statement

Jiaxiang Li: Writing – original draft, Visualization, Validation, Software, Resources, Methodology, Investigation, Formal analysis, Data curation, Conceptualization. **John Kaiser Calautit:** Writing – review & editing, Supervision, Software, Methodology. **Carlos Jimenez-Bescos:** Writing – review & editing, Supervision.

Declaration of competing interest

The authors declare the following financial interests/personal relationships which may be considered as potential competing interests: Jiaxiang Li has patent licensed to 202222823936.7.

Data availability

The data that has been used is confidential.

Acknowledgement

Thanks to the support of Dalian Meizhu Furniture Co., Ltd for the assistance in making the experiment model and providing the test space. The technology described here is licensed with reference number ZL 202222823936.7.

Appendix

Table A1
Wind speed profile based on the experimental testing of double height single fin model (0.1 mm fins/0.91g per fin), wind from face direction (0° wind), in Figure (9a)

Average wind speed (m/s)	Front fin open angle (°)	Wind speed profile function (m/s)
2.50	21	$v = -35.79 \times r^2 + 5.41 \times r + 2.49$
2.21	20.6	$v = -21.44 \times r^2 + 2.87 \times r + 2.24$
1.80	18.4	$v = -18.31 \times r^2 + 2.03 \times r + 1.88$
1.64	17.5	$v = -24.99 \times r^2 + 4.1 \times r + 1.60$
1.34	14.5	$v = -15.16 \times r^2 + 1.23 \times r + 1.47$
1.10	10.8	$v = -10.28 \times r^2 + 0.94 \times r + 1.17$
0.81	8.1	$v = -1.33 \times r^2 - 10.2 \times r + 0.96$
0.61	6.7	$v = -0.14 \times r^2 - 0.97 \times r + 0.73$

Table A2
Wind speed profile based on the experimental testing of double height single fin model (0.1 mm fins/0.91g per fin), wind from edge direction (22.5° wind), in Figure (9b)

Average wind speed (m/s)	Fin open angle 1 (°)	Fin open angle 2 (°)	Wind speed profile function (m/s)
2.34	12	13	$v = -43.02 \times r^2 + 6.50 \times r + 2.40$
2.03	10	12	$v = -38.37 \times r^2 + 6.36 \times r + 2.05$
1.81	9	11	$v = -14.79 \times r^2 + 0.52 \times r + 2.06$
1.63	8	10	$v = -19.25 \times r^2 + 1.55 \times r + 1.83$
1.39	7	9.	$v = -14.75 \times r^2 + 1.25 \times r + 1.56$
1.06	6	8	$v = -9.54 \times r^2 + 0.04 \times r + 1.24$
0.80	5	7	$v = -12.34 \times r^2 + 1.55 \times r + 0.84$
0.60	4.	6	$v = -3.85 \times r^2 + 0.07 \times r + 0.67$

Fig. A1. Field test experiment photo

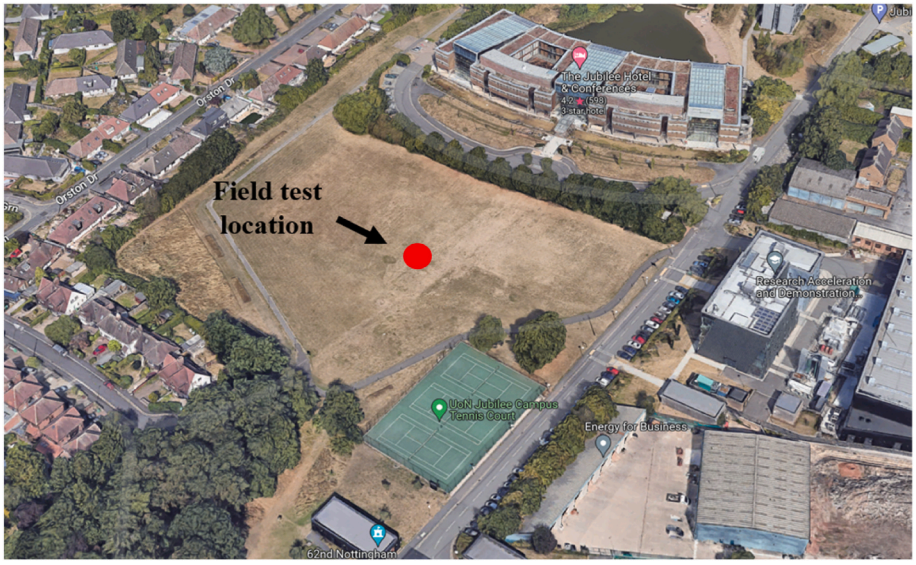

Fig. A2. Field test location

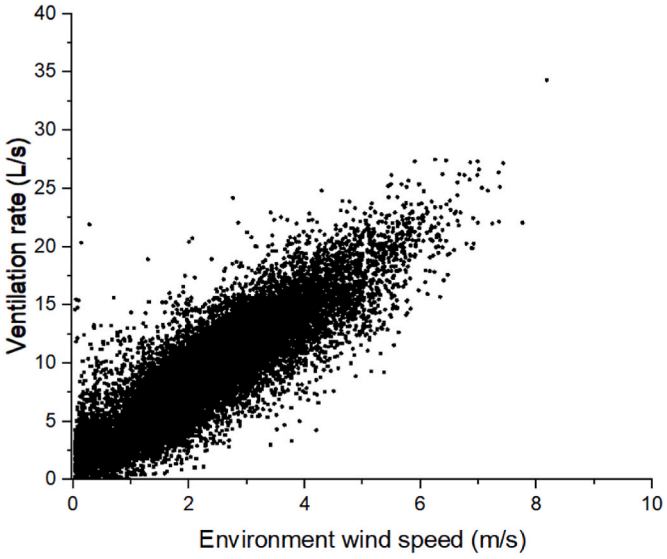

Fig. A3. Field test results of the ventilation rate to environment wind speed raw data in L/s

References

[1] B.-j. He, et al., Overview of rural building energy efficiency in China, Energy Pol. 69 (2014) 385–396.
[2] L. Pérez-Lombard, J. Ortiz, C. Pout, A review on buildings energy consumption information, Energy Build. 40 (3) (2008) 394–398.
[3] P. Liu, M. Justo Alonso, H.M. Mathisen, Heat recovery ventilation design limitations due to LHC for different ventilation strategies in ZEB, Build. Environ. 224 (2022), 109542.
[4] IEA, The Future of Cooling-Opportunities for Energy-Efficient Air Conditioning, 2018.
[5] H.-Y. Chan, S.B. Riffat, J. Zhu, Review of passive solar heating and cooling technologies, Renew. Sustain. Energy Rev. 14 (2) (2010) 781–789.
[6] J. Li, et al., Evaluating the energy-saving potential of earth-air heat exchanger (EAHX) for Passivhaus standard buildings in different climates in China, Energy Build. (2023), 113005.
[7] F. Jomehzadeh, et al., Natural ventilation by windcatcher (Badgir): a review on the impacts of geometry, microclimate and macroclimate, Energy Build. 226 (2020), 110396.
[8] N.Z. Ghalam, M. Farrokhzad, H. Nazif, Investigation of optimal natural ventilation in residential complexes design for temperate and humid climates, Sustainable Energy, Grids and Networks 27 (2021), 100500.
[9] N. Nasrollahi, P. Ghobadi, Field measurement and numerical investigation of natural cross-ventilation in high-rise buildings; Thermal comfort analysis, Appl. Therm. Eng. 211 (2022), 118500.
[10] E. Bay, A. Martinez-Molina, W.A. Dupont, Assessment of natural ventilation strategies in historical buildings in a hot and humid climate using energy and CFD simulations, J. Build. Eng. 51 (2022), 104287.
[11] H. Zhang, et al., A critical review of combined natural ventilation techniques in sustainable buildings, Renew. Sustain. Energy Rev. 141 (2021), 110795.
[12] K. Bamdad, et al., Introducing extended natural ventilation index for buildings under the present and future changing climates, Build. Environ. (2022), 109688.
[13] P.K. Sangdeh, N. Nasrollahi, Windcatchers and their applications in contemporary architecture, Energy and Built Environment 3 (1) (2022) 56–72.
[14] Y. He, et al., Experimental and CFD study of ventilation performance enhanced by roof window and mechanical ventilation system with different design strategies, Build. Environ. 224 (2022), 109566.
[15] H. Montazeri, R. Azizian, Experimental study on natural ventilation performance of one-sided wind catcher, Build. Environ. 43 (12) (2008) 2193–2202.
[16] W. Pan, et al., A model for calculating single-sided natural ventilation rate in an urban residential apartment, Build. Environ. 147 (2019) 372–381.
[17] B. Zhang, et al., Turbulence-induced ventilation of an isolated building: ventilation route identification using spectral proper orthogonal decomposition, Build. Environ. 223 (2022), 109471.
[18] M. Farouk, Comparative study of hexagon & square windcatchers using CFD simulations, J. Build. Eng. (2020) 31.
[19] S. Jafari, V. Kalantar, Numerical simulation of natural ventilation with passive cooling by diagonal solar chimneys and windcatcher and water spray system in a hot and dry climate, Energy Build. 256 (2022), 111714.
[20] M. Ghoulem, et al., Analysis of passive downdraught evaporative cooling windcatcher for greenhouses in hot climatic conditions: parametric study and impact of neighbouring structures, Biosyst. Eng. 197 (2020) 105–121.
[21] A. Noroozi, Y. Veneris, Thermal assessment of a novel combine evaporative cooling wind catcher, Energies 11 (2018) 442.
[22] L. Moosavi, et al., New design for solar chimney with integrated windcatcher for space cooling and ventilation, Build. Environ. 181 (2020), 106785.
[23] X. Morales, et al., Thermal effectiveness of wind-tower with heated exit-wall and inlet-air humidification: effects of winter and summertime, Build. Environ. 204 (2021), 108110.
[24] Z.M. Gilvaei, A.H. Poshtiri, A.M. Akbarpoor, A novel passive system for providing natural ventilation and passive cooling: evaluating thermal comfort and building energy, Renew. Energy. 198 (2022) 463–483.
[25] K. Pelletier, J. Calautit, Analysis of the performance of an integrated multistage helical coil heat transfer device and passive cooling windcatcher for buildings in hot climates, J. Build. Eng. 48 (2022), 103899.
[26] Y. Jiang, Q. Chen, Effect of fluctuating wind direction on cross natural ventilation in buildings from large eddy simulation, Build. Environ. 37 (4) (2002) 379–386.
[27] N. Kumar, et al., Parametric study on vertical void configurations for improving ventilation performance in the mid-rise apartment building, Build. Environ. 215 (2022), 108969.
[28] J.K. Calautit, et al., Numerical and experimental investigation of the indoor air quality and thermal comfort performance of a low energy cooling windcatcher with heat pipes and extended surfaces, Renew. Energy 145 (2020) 744–756.
[29] J.P. Harrouz, K. Ghali, N. Ghaddar, Integrated solar – windcatcher with dew-point indirect evaporative cooler for classrooms, Appl. Therm. Eng. 188 (2021), 116654.
[30] H. Montazeri, et al., Two-sided wind catcher performance evaluation using experimental, numerical and analytical modeling, Renew. Energy 35 (7) (2010) 1424–1435.
[31] M. Liu, C. Jimenez-Bescos, J. Calautit, CFD investigation of a natural ventilation wind tower system with solid tube banks heat recovery for mild-cold climate, J. Build. Eng. 45 (2022), 103570.
[32] H. Mahon, D. Friedrich, B. Hughes, Wind tunnel test and numerical study of a multi-sided wind tower with horizontal heat pipes, Energy 260 (2022), 125118.
[33] N. Khan, Y. Su, S.B. Riffat, A review on wind driven ventilation techniques, Energy Build. 40 (8) (2008) 1586–1604.
[34] L.O. Adekoya, Wind energy end-use: the performance characteristics of a rotating suction cowl, Renew. Energy 2 (4) (1992) 385–389.
[35] P. Nejat, et al., Passive cooling and natural ventilation by the windcatcher (Badgir): an experimental and simulation study of indoor air quality, thermal comfort and passive cooling power, J. Build. Eng. 41 (2021), 102436.
[36] J. Li, et al., Experimental and numerical evaluation of a novel dual-channel windcatcher with a rotary scoop for energy-saving technology integration, Build. Environ. (2023), 110018.
[37] Z. Moghtader Gilvaei, A. Haghighi Poshtiri, A. Mirzazade Akbarpoor, A novel passive system for providing natural ventilation and passive cooling: evaluating thermal comfort and building energy, Renew. Energy 198 (2022) 463–483.
[38] J. Foroozesh, et al., CFD modeling of the building integrated with a novel design of a one-sided wind-catcher with water spray: focus on thermal comfort, Sustain. Energy Technol. Assessments 53 (2022), 102736.
[39] M. Ghoulem, et al., Design of a passive downdraught evaporative cooling windcatcher (PDEC-WC) system for greenhouses in hot climates, Energies 13 (2020) 2934.
[40] M. Afshin, et al., An experimental study on the evaluation of natural ventilation performance of a two-sided wind-catcher for various wind angles, Renew. Energy 85 (2016) 1068–1078.

[41] L. Li, C.M. Mak, The assessment of the performance of a windcatcher system using computational fluid dynamics, Build. Environ. 42 (3) (2007) 1135–1141.
[42] B.M. Jones, R. Kirby, Quantifying the performance of a top–down natural ventilation Windcatcher, Build. Environ. 44 (9) (2009) 1925–1934.
[43] J.K. Calautit, D. O'Connor, B.R. Hughes, A natural ventilation wind tower with heat pipe heat recovery for cold climates, Renew. Energy 87 (2016) 1088–1104.
[44] J.K. Calautit, et al., Development of a natural ventilation windcatcher with passive heat recovery wheel for mild-cold climates: CFD and experimental analysis, Renew. Energy 160 (2020) 465–482.
[45] M. Farouk, Comparative study of hexagon & square windcatchers using CFD simulations, J. Build. Eng. 31 (2020), 101366.
[46] P.V. Dorizas, et al., Performance of a natural ventilation system with heat recovery in UK classrooms: an experimental study, Energy Build. 179 (2018) 278–291.
[47] P. Nejat, et al., Anti-short-circuit device: a new solution for short-circuiting in windcatcher and improvement of natural ventilation performance, Build. Environ. 105 (2016) 24–39.
[48] J.H. Bell, R.D. Mehta, Design and Calibration of the Mixing Layer and Wind Tunnel, 1989.
[49] S. Kirk, M. Kolokotroni, Windcatchers in modern UK buildings: experimental study, Int. J. Vent. 3 (1) (2004) 67–78.
[50] P.S. Charlesworth, Air Exchange Rate and Airtightness Measurement Techniques - an Application Guide, Coventry: Air Infiltration and Ventilation Centre, 1988.
[51] B. Blocken, et al., Computational analysis of the performance of a venturi-shaped roof for natural ventilation: venturi-effect versus wind-blocking effect, Comput. Fluid 48 (1) (2011) 202–213.
[52] T. Kobayashi, et al., Numerical analysis of wind-induced natural ventilation for an isolated cubic room with two openings under small mean wind pressure difference, Build. Environ. (2022), 109694.
[53] B.R. Hughes, J.K. Calautit, S.A. Ghani, The development of commercial wind towers for natural ventilation: a review, Appl. Energy 92 (2012) 606–627.
[54] J.K. Calautit, B.R. Hughes, Wind tunnel and CFD study of the natural ventilation performance of a commercial multi-directional wind tower, Build. Environ. 80 (2014) 71–83.
[55] J.K. Calautit, B.R. Hughes, Measurement and prediction of the indoor airflow in a room ventilated with a commercial wind tower, Energy Build. 84 (2014) 367–377.